



Isotopic Probe Illuminates the Role of the Electrode Surface in Proton Coupled Hydride Transfer Electrochemical Reduction of Pyridinium on Pt(111)

Elizabeth L. Zeitler,^a Mehmed Z. Ertem,^{b,c} James E. Pander III,^a Yong Yan,^a Victor S. Batista,^{c,z} and Andrew B. Bocarsly^{a,*,z}

^aDepartment of Chemistry, Princeton University, Princeton, New Jersey 08544, USA

^bChemistry Department, Brookhaven National Laboratory, Upton, New York 11973, USA

^cDepartment of Chemistry, Yale University, New Haven, Connecticut 06520, USA

A recently proposed mechanism for electrochemical CO₂ reduction on Pt (111) catalyzed by aqueous acidic pyridine solutions suggests that the observed redox potential of ca. -600 mV vs. SCE is due to the one-electron reduction of pyridinium through proton coupled electron transfer (PCET) to form H atoms adsorbed on the Pt surface (H_{ads}). The initial pyridinium reduction was probed isotopically via deuterium substitution. A combined experimental and theoretical analysis found equilibrium isotope effects (EIE) due to deuterium substitution at the acidic pyridinium site. A shift in the cathodic cyclic voltammetric half wave potential of -25 mV was observed, consistent with the theoretical prediction of -40 mV based on the recently proposed reaction mechanism where pyridinium is essential to establish a high concentration of Bronsted acid in contact with the substrate CO₂ and with the Pt surface. A prefeature in the cyclic voltammogram was examined under isotopic substitution and indicated an H_{ads} intermediate in pyridinium reduction. Theoretical prediction and observation of an EIE supported the assignment of the cathodic wave to the proposed reduction of pyridinium through PCET forming H_{ads} and eventually H₂ on the Pt surface.

© The Author(s) 2015. Published by ECS. This is an open access article distributed under the terms of the Creative Commons Attribution Non-Commercial No Derivatives 4.0 License (CC BY-NC-ND, <http://creativecommons.org/licenses/by-nc-nd/4.0/>), which permits non-commercial reuse, distribution, and reproduction in any medium, provided the original work is not changed in any way and is properly cited. For permission for commercial reuse, please email: oa@electrochem.org. [DOI: 10.1149/2.0821514jcs] All rights reserved.

Manuscript submitted September 8, 2015; revised manuscript received October 9, 2015. Published October 21, 2015.

Efficient and quantitative reduction of carbon dioxide to interesting or useful chemicals is challenging and is under vigorous investigation.¹⁻³ Electrochemical reduction of carbon dioxide has the unique advantage of direct applied potential control over the energy of one of the reactants, the electron, however the overpotential required for reduction remains high at many electrochemical interfaces. This fact indicates that electrode surfaces as catalysts either do not significantly lower the activation barrier for CO₂ reduction or proceed through high energy intermediates. In order to provide lower energy pathways to CO₂ reduction and pursue mechanistic understanding, solution based catalysts have been employed.^{2,4,5} Pyridinium (PyrH⁺) catalyzes the electrochemical reduction of CO₂ to methanol and formic acid at a platinum (Pt) electrode at low overpotentials (ca. -600 mV vs. SCE).^{6,7} The mechanism of CO₂ reduction was proposed to initiate with the electrochemical reduction of PyrH⁺. Originally it was believed that this reduction proceeded through the ring π* system generating a pyridinyl radical.^{6,7} This radical was postulated to bind CO₂, forming the active intermediate in the electron transfer to CO₂.⁸ Evidence for the proposed mechanism included digital simulation of the cyclic voltammetric scan rate dependence on a Pt electrode, an observed first order dependence of current on concentrations of both PyrH⁺ and CO₂, as well as density functional theory (DFT) calculations.^{6,8,9} Reduction of CO₂ to methanol has also been observed photochemically in the presence of PyrH⁺, indicating that PyrH⁺ reduction may be possible in homogeneous solution using a photocatalyst with suitably negative excited state redox potentials,¹⁰ as had been indicated by quenching measurements.¹¹ Additionally, a vibrational spectrum indicative of carbamate formation has been observed in the gas phase upon reaction of CO₂^{•-} with pyridine.¹² More recent work suggests that pyridinium reduction involves the acidic proton not the ring system.¹¹

The assignment of the reduction at approximately -600 mV vs. SCE to the formation of pyridinyl radical was initially challenged by computational studies that indicated a significantly more negative reduction potential for PyrH⁺ than that observed at a Pt

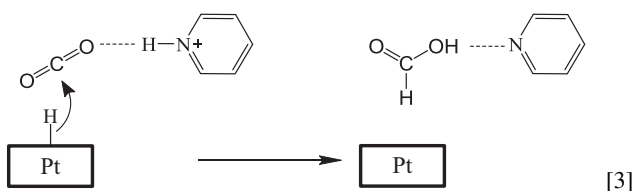
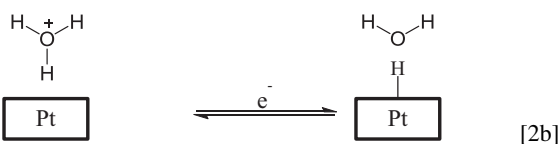
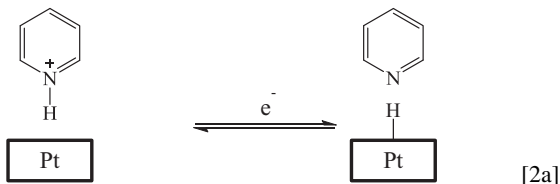
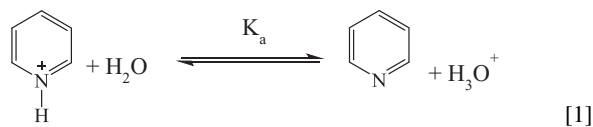
electrode.^{13,14} In response to this discrepancy, several other mechanistic pathways were proposed for the initial reduction of PyrH⁺ and subsequent reduction of CO₂, including two electron reduction of PyrH⁺ to dihydropyridine,¹⁴ assisted deprotonation of pyridinyl via a hydrogen bound intermediate,¹⁵ and specific adsorption of PyrH⁺ or pyridinyl.^{13,15} However these possible reaction mechanisms did not find experimental support when a Pt electrode was employed.^{11,16} Pyridinium reduction has recently been explored at other electrode surfaces, including Ir and Au.^{17,18} In the case of Au, specific adsorption of pyridinium is implicated, and for Ir the formation of pyridyl as a primary reduction product does not appear to be supported.

Another mechanism that has been proposed for the electrocatalytic reduction of CO₂ to methanol, in the presence of PyrH⁺ on a Pt electrode, involves the initial generation of PyrH⁺ through a pre-equilibrium between Pyr and PyrH⁺ at pH = 5.2 (Eq. 1), followed by 1e⁻ reduction of PyrH⁺ on the Pt(111) surface to generate adsorbed hydrogen atoms (H_{ads}) on the electrode (Eq. 2).¹⁹ Finally, electrophilic attack of CO₂ on H_{ads} causes a hydride ion transfer, which is facilitated by PyrH⁺ acting as a proton donor (Eq. 3).¹⁹ The net effect of the reaction sequence is a proton coupled hydride transfer (PCHT). There is an important subtlety in this reaction scheme. Namely, that an aqueous electrolyte composed of a weak acid provides two sources of protons: hydronium via Equation 2b and the weak acid itself (pyridinium in Equations 1 and 2a). If Equation 1 presents a rapid equilibrium, then in fact protons are delivered from only one source. That is both sides of Equation 1 provide protons and those protons are reduced at the electrode surface at a rate that is slow compared to the equilibration rate represented in this equation. Thus, there is a time averaged proton environment at the electrode interface, and at the point of reduction either acid source may be supplying the proton. As the rate of proton reduction increases with respect to the rate of hydrogen exchange, however, either Equation 2a or the direct reduction of H₃O⁺ Equation 2b can dominate the reaction. This issue is not only of interest in the case of pyridinium reduction that is evaluated here, but is of general interest with regard to weak acid reductions. Currently, reaction branching of this type is an open question for a number of electrochemical reactions that incorporate

*Electrochemical Society Active Member.

^zE-mail: bocarsly@princeton.edu; victor.batista@yale.edu

proton reduction.



Platinum is unique in providing a catalytic surface for reduction reactions of protons. Additionally, PyrH^+ and other weak acids have been found to reduce at more modest potentials at Pt cathodes than at other electrode materials. Reductive hydrogen atom adsorption from strong and weak acid solutions at Pt electrodes has been investigated and has been observed in steady state voltammetry at a microdisk electrode,²⁰ in sum frequency generation IR spectroscopy²¹ and in surface enhanced Raman spectroscopy.²² Specifically, under potential deposition (UPD) of a monolayer of strongly adsorbed hydrogen from H_3O^+ is well established on Pt surfaces.^{23–28} At the potentials under consideration in this work, an UPD hydrogen monolayer is expected to be present on (111) facets of the Pt electrode surface at three fold fcc sites.^{29,30} At the H_2/H^+ redox potential, a submonolayer of more weakly adsorbed hydrogen atoms (OPD H) is formed in an on top configuration, from which hydrogen evolution has been attributed.³¹ In addition, PyrH^+ reduction to H_{ads} on Pt and pyridine has been previously suggested in a study of dissociation of weak acids.³² The proposed mechanism of PyrH^+ reduction on Pt electrode surfaces has further support from an examination undertaken by the Bocarsly group of the dependence of weak acid standard redox potentials on $\text{p}K_a$ for a series of acids reduced at a Pt electrode¹¹ which has recently been confirmed in a study of PyrH^+ and weak acid proton reduction on Pt.¹⁶

Proton coupled electron transfer (PCET) mechanisms such as that proposed in Equation 2 are anticipated to exhibit isotope effects upon substitution of the acidic hydrogen by deuterium. Substitution by the heavier isotope is expected to affect the current in cyclic voltammetry via change in the diffusion coefficient upon deuteration. Deuteration also affects the reaction thermodynamics via change in the free energy of the acid dissociation equilibrium resulting from the changes in zero point energy (ZPE) and entropy of the deuterated versus protonated acid.³³ The change in zero point energy upon deuteration will be greater in bonds where the X-H or X-D bond is stronger. This greater stabilization favors deuterium equilibration into the more tightly bound state. An N-H bond is more tightly bound than a Pt-H bond, and thus in an N-H to Pt-H PCET, deuterium substitution would be expected to favor reactants, leading to a normal equilibrium isotope effect (EIE). In this study, the observed isotope effect combined with the theoretical analysis provide evidence of the breaking of the N-H bond during PyrH^+ reduction, in agreement with the recently proposed mechanism for electrocatalytic reduction of CO_2 via platinum hydride formation in the presence PyrH^+ .

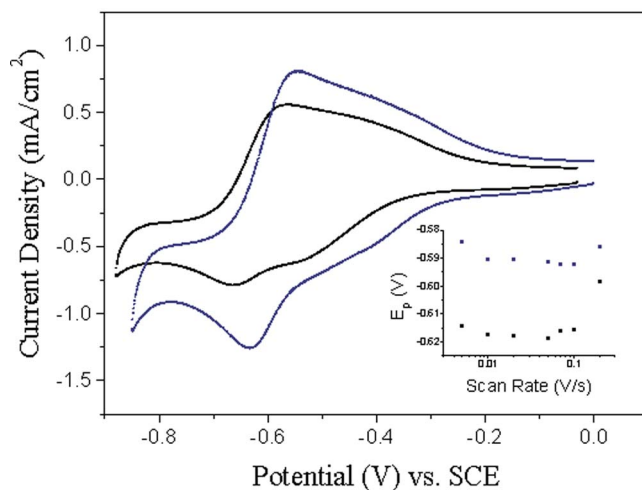


Figure 1. Cyclic voltammograms (CV) of pyridinium 10 mM aqueous solution (at pH or pD = 3.0) in H_2O (gray) and D_2O (black) taken at 100 mV/s, showing a shift in the half-wave potential for reduction upon deuteration. Inset is the half wave potentials plotted over log scan rate for D_2O (black) and H_2O (gray).

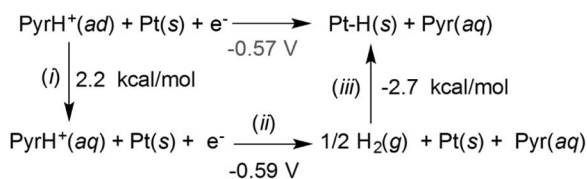
Results and Discussion

Figure 1 shows that the reduction of PyrH^+ at pH 3.0 in aqueous KCl solution produces a cyclic voltammogram wave with an invariant half-wave potential $E_{1/2} = -0.590 \pm 0.002$ V vs. SCE, over scan rates of 5–200 mV/s. The scan rate range was chosen where the peak to peak separation was less than 100 mV, indicating no complications from a prefeature observed in acid reductions on Pt.¹¹ In Figure 1, an additional reduction process was observed at approximately -0.42 V vs. SCE and was attributed to reduction of H_3O^+ from water due to a proton concentration in the bulk of 1 mM at pH = 3.0. The reduction of protons derived from water and that derived from PyrH^+ at a platinum cathode can be described as proton reduction to H_2 where the formal potential for any acid, $E_0^{\prime \text{HA}/\text{H}_2}$, is simply that for proton reduction $E_0^{\prime \text{H}_3\text{O}^+/\text{H}_2}$ modulated by the acid dissociation constant K_a , of HA Equation 4.^{11,32}

$$E_0^{\prime \text{HA}/\text{H}_2} = E_0^{\prime \text{H}_3\text{O}^+/\text{H}_2} + \frac{RT}{F} \ln K_a \quad [4]$$

The formal potential is the thermodynamic standard potential modulated by experimental conditions such as ionic strength and solvent medium. As already noted, weak acids often dissociate before reduction. This process has been documented on platinum disk microelectrodes,^{34,35} suggesting that proton reduction from hydronium is the likely process in either direct hydronium or PyrH^+ reduction cases. Using the relationship in Equation 4 and approximating hydronium and PyrH^+ reduction as reversible over the scan rates chosen so that the formal potential, $E_0^{\prime \text{HA}/\text{H}_2} \cong E_{1/2}$, the $E_{1/2}$ values calculated for hydronium and PyrH^+ protons are estimated to be -0.42 V vs. SCE and -0.55 V vs. SCE, close to that observed experimentally.

We performed density functional theory (DFT) calculations at PBE level of theory³⁶ (see supporting information for details) to compute the overall free energy change for the reduction of PyrH^+ on Pt(111) surface, as obtained by summing the free energy changes of the three elementary steps in the thermodynamic cycle given in Scheme 1.¹⁹ Scheme 1, ii represents the net reaction proposed to be occurring in the cyclic voltammetry under an Ar atmosphere, which is in good agreement with the observed reduction potential of -0.59 V vs. SCE. It also is interesting to examine the calculated energies for formation of Pt-H, the proposed active intermediate. The reduction potential of adsorbed PyrH^+ to form Pt-H on Pt(111) (Scheme 1) was calculated



Scheme I. Thermodynamic cycle (i)–(iii) used to obtain the free energy change due to the overall reaction where PyrH^+ is reduced to hydrogen adsorbed on the Pt surface.

to be -0.57 V vs. SCE which is also in good agreement with the reduction potential observed by cyclic voltammetry (CV) experiments.

Cyclic voltammetry and DFT calculations were performed to understand the effect of deuteration on the reduction of PyrD^+ at Pt(111). In deuterated electrolyte, the half-wave potential for PyrH^+ reduction was also invariant, but it was shifted to -0.614 ± 0.005 V vs. SCE, a change in $\Delta E_{1/2} = -25$ mV relative to the non-deuterated electrolyte. Similar to the potential shift observed for acids of different strengths, the observed potential shift for PyrH^+ vs. PyrD^+ can be attributed to an increase in the free energy demand for deprotonation of PyrH^+ of approximately $+0.4$ pK_a units under deuteration (Table I).³⁷ The effective change in pK_a of acids upon deuteration was reported very soon after the discovery of deuterium.^{38–40} Increases in pK_a of approximately 0.5 units for deuterated vs. undeuterated acids were observed with weaker organic acids exhibiting greater shifts.⁴¹ Simple substitution of the EIE on K_a into Equation 4 indicates that a shift in 0.4 pK_a units produces a change in redox potential of -23 mV, close to the -25 mV observed experimentally. Incorporation of $E_0^{D_3O^+/D_2} = -0.013$ V into Equation 4 results in a final $\Delta E_{1/2}^{\text{D-H}}$ calculated from experimental parameters for PyrH^+ of -0.36 V. Significantly, other weak acids exhibit similar equilibrium isotope shifts in cyclic voltammetry half wave potential with deuteration of the exchangeable position (Table I). A plot of cyclic voltammetric half wave potential vs. pK_{a(D)} results in Equation 5.

$$E_{1/2} = -0.061 \times pK_{a(D)} - 0.26 \quad [5]$$

Similar to the empirical equation for protonated weak acids,¹¹ the rate of change in cyclic voltammetric potential with pK_a was 61 ± 6 mV, close to 59 mV as predicted by the Nernst equation, and the intercept was 0.26 ± 0.04 V, close to the standard potential of $\text{D}_3\text{O}^+/\text{D}_2$. It is generally regarded that the mechanism for proton reduction at platinum electrodes involves a surface bound platinum hydride. Table I shows that weak acids of varying structure experience a similar shift in half-wave potential upon substitution of the acidic proton with a deuteron. An identical shift is observed between the H_3O^+ and D_3O^+ systems. Because the shift in half-wave potential is invariant with the structure of the molecule delivering the proton, it can be inferred that these reactions proceed by a similar mechanism. Thus, we invoke a surface H_{ads} intermediate for weak acid reduction at a platinum electrode.

In addition, a shift of -40 mV was found for the reduction potential of PyrD^+ relative to PyrH^+ in process ii, corresponding to a free energy

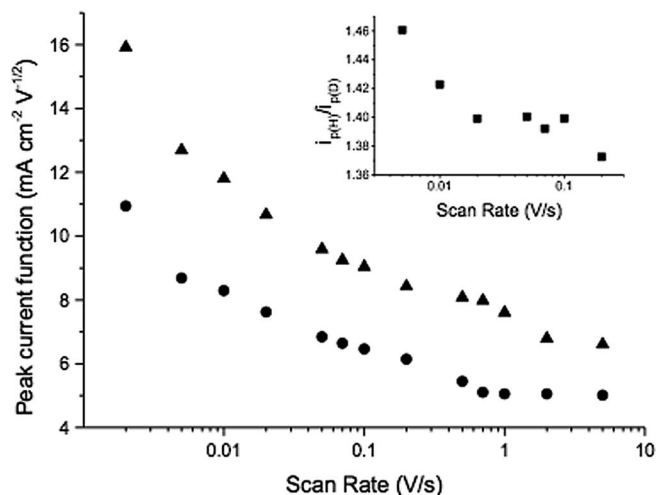


Figure 2. Pyridinium reductive peak current function ($i_p/v^{1/2}$) vs. scan rate for protonated solution (triangles) and deuterated solution (circles) at pH or pH* = 3.0. The protonated peak current is uniformly greater than the deuterated current, with the ratio of peak currents shown in the inset.

change of $0.9 \text{ kcal mol}^{-1}$, determined by changes in zero point energies and entropic contributions obtained via periodic DFT calculations. These computational results are consistent with the experimentally observed shift of the reduction potential of -25 mV, supporting the assignment of the reductive wave to the 1e^- reduction of PyrH^+ to H_{ads} and ultimately H_2 on the Pt(111) electrode surface.

To investigate if the shift in the reduction potential can be produced by changes in the chemical equilibrium of PyrH^+ induced by deuteration of non-exchangeable positions, the reduction potential of d_5 -pyridinium in water was measured by scan rate dependent cyclic voltammetry. A 10 mV shift of the potential of PyrH^+ reduction was observed which is significantly smaller than the shift observed upon deuteration of PyrH^+ at the exchangeable (nitrogen) position. Our observations are consistent with equilibrium isotope effects of similar magnitude determined electrochemically for naphthalene- h_8/d_8 and anthracene- $\text{h}_{10}/\text{d}_{10}$ in THF, with shifts of -13 and -12 mV respectively.⁴³ The greater isotope shift of ~ -25 mV, observed for h_5 - PyrD^+ in D_2O , is consistent with the participation of an exchangeable proton in the reduction half reaction and further rules out direct charge transfer to the ring π -system, which would lead to an isotopic shift of half size observed based on the results reported above.

Figure 2 shows the peak current density vs. scan rate for deuterated and protonated solutions at pH or pH* = 3.0. Under these conditions, PyrH^+ should be $>99\%$ protonated/deuterated. Peak current in a cyclic voltammogram (Equation 6), when divided by the square root of the scan rate ($i_p/v^{1/2}$) to yield the peak current function, gives a measure of the resulting reaction rate after removing the time dependence associated with diffusion of the reactant(s) to the electrode

Table I. Half wave potential for reduction of various weak acids at a Pt electrode in D_2O and H_2O electrolytes from our cyclic voltammetry, literature pK_{a(H)}⁴² and our calculated pK_{a(D)} values (Supporting Information).³⁷ Errors for measured $E_{1/2}$ values were taken as the 95% confidence interval from the mean $E_{1/2}$ taken from 5–200 mV/s.

Acid	pK _{a(H)}	pK _{a(D)}	$\Delta pK_{a(D-H)}$	$E_{1/2 \text{ H}}$ (V vs. SCE)	$E_{1/2 \text{ D}}$ (V vs. SCE)	$\Delta E_{1/2 \text{ (D-H)}}$ Exp. (V)	$\Delta E_0^{\text{(D-H)}}$ (V) calc. from $\Delta pK_{a(D-H)}$, $\Delta E_0^{\text{H}_3\text{O}^+/\text{H}_2}$ and Eq. 4
2,6-lutidinium	6.70	7.21	0.51	-0.680 ± 0.001	-0.702 ± 0.001	-0.022 ± 0.002	-0.043
4-methyl pyridinium	5.99	6.45	0.46	-0.629 ± 0.002	-0.662 ± 0.001	-0.032 ± 0.003	-0.040
Pyridinium	5.23	5.63	0.40	-0.590 ± 0.002	-0.614 ± 0.005	-0.025 ± 0.007	-0.036
Acetic acid	4.756	5.12	0.36	-0.554 ± 0.003	-0.577 ± 0.001	-0.023 ± 0.004	-0.034
Benzoic acid	4.204	4.52	0.32	-0.511 ± 0.001	-0.538 ± 0.002	-0.023 ± 0.003	-0.032

surface.⁴⁴

$$i_p = 2.69 \times 10^5 n^{3/2} AC_O^* D^{1/2} \nu^{1/2} \quad [6]$$

The peak current function should be independent of the scan rate for a reversible electron transfer without coupled chemical steps according to Equation 6. However, as shown in Fig. 2, we observed that the peak current for both deuterated and protonated electrolytes increased at low scan rates, suggesting that there is a slow chemical step coupled to PyrH⁺ reduction.⁴⁴

The ratio $i_{p(H)}/i_{p(D)}$ can reflect changes in the diffusion coefficient induced by deuteration. The diffusion coefficients for PyrD⁺ and PyrH⁺ were calculated from combined cyclic and rotating disk voltammetric studies (see supporting information). The diffusion coefficient for PyrH⁺, D_{PyrH^+} , in 0.5 M KCl has been reported to be $2.1 \times 10^{-5} \text{ cm}^2 \text{ s}^{-1}$ using this method.¹¹ The number of electrons transferred and calculated diffusion coefficient for PyrD⁺ from combined cyclic voltammetric and rotating disk studies is $n = 0.9 \pm 0.1$ and $D_{\text{PyrD}^+} = 9.4 \times 10^{-6} \pm 5 \times 10^{-6} \text{ cm}^2 \text{ s}^{-1}$ respectively (Figure S1). This results in a value of 2.2 for $D_{\text{PyrH}^+}/D_{\text{PyrD}^+}$. Given that the rotating disk data confirms that $n = 1$, the ratio $D_{\text{PyrH}^+}/D_{\text{PyrD}^+}$ can also be obtained from the ratio of the squares of the peak cyclic voltammetric currents observed for PyrH⁺ vs. PyrD⁺. The necessary data is provided in Figure 2 and produces a value for $D_{\text{PyrH}^+}/D_{\text{PyrD}^+}$ of 2.1 ± 0.1 confirming the result of the RDE experiment. Similarly, diffusion coefficients for D₃O⁺ in D₂O and H₃O⁺ in H₂O have been reported to be $6.7 \times 10^{-5} \text{ cm}^2 \text{ s}^{-1}$ and $9.3 \times 10^{-5} \text{ cm}^2 \text{ s}^{-1}$, respectively at infinite dilution, leading to a ratio of $D_{\text{H}^+}/D_{\text{D}^+} = 1.4$.^{45,46} In solutions of increasing ionic strength up to 0.5 M KCl solutions, the ratio of diffusion coefficients for $D_{\text{H}^+}/D_{\text{D}^+}$ has been reported to be between 1.4 and 1.8.^{45,46} The ratio of peak currents for proton and deuteron reduction at a platinum electrode, $i_{\text{H}}/i_{\text{D}}$, was measured and found to be 1.2 (Table S1). Squaring the current ratio leads to a projected diffusion coefficient ratio of $1.4 (\pm 0.1)$ for $D_{\text{H}^+}/D_{\text{D}^+}$, the same as observed in the reported studies. Thus, both the pyridinium and hydronium data indicate that for H and D, peak current ratios can be explained by the change in diffusion coefficient upon deuteration. Overall the pyridinium related diffusion coefficients are smaller (~20%) than the hydronium diffusion coefficients as expected for a process that is limited by simple diffusion versus proton hopping. The isotopic (H/D) ratios of hydronium diffusion coefficients (1.4) versus pyridinium diffusion coefficients (2.1) are statistically different at the 95% confidence level. This is consistent with pyridine acting as a “proton shuttle” that brings this species up to the electrode reaction zone. However, given that proton exchange between pyridine and water is expected to be rapid, no conclusions can be drawn about the nature of the protonic species undergoing the reduction associated with the cyclic voltammetric wave centered at -0.59 V vs. SCE . However, it is interesting to note that the quantum mechanical analysis presented here, which assumes that the absorbing species undergoing reduction is pyridinium (not hydronium) produces a model that is consistent with the data presented here.

As already noted the existence of a surface adsorbed hydrogen intermediate is well documented in the reduction of hydronium (generated by a strong acid) by both electrochemical measurements and spectroelectrochemical observations. However, the explicit observation of a surface platinum hydride has not been well documented for weak acids at moderate pHs. However, we find a very distinctive feature in the cyclic voltammetric response of pyridinium at platinum electrodes that we directly correlate with the existence of a surface platinum hydride intermediate. As shown in Figure 3, at scan rates above ~200 mV/s a distinctive prefeature exists leading to a distortion of the positive potential side of the pyridinium wave. At slow scan rates (up to 100 mV/s), the voltammetry appears reversible. Analysis of this voltammetric feature is complicated by the extensive convolution of the prewave with the diffusive peak at slow to moderate scan rate. In order to deconvolute the distorted wave into the diffusive wave and this peak, a wave with reversible behavior was subtracted from the distorted wave. This was achieved by scaling a slow scan rate (where

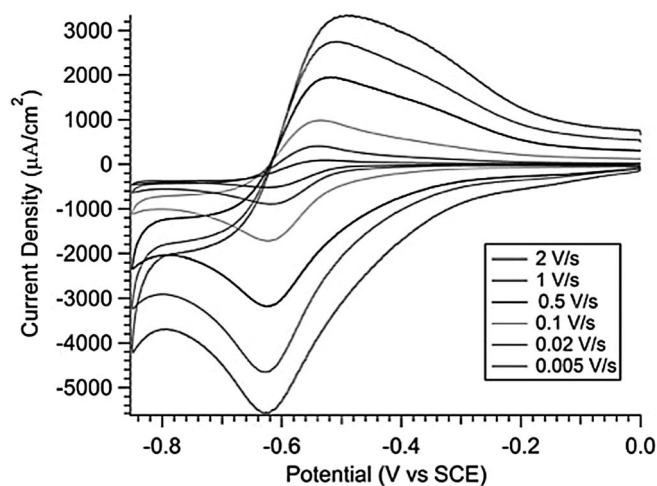


Figure 3. Scan rate dependence of the cyclic voltammetric response of 10 mM pyridine, pH 5.1 at a platinum working electrode in aqueous KCl solution. At fast scan rates, the electrochemical behavior noticeably deviates from reversibility.

the electrochemical behavior appears to be reversible) by the constant factor $\sqrt{\frac{\nu_{\text{fast}}}{\nu_{\text{slow}}}}$ to simulate the voltammetric response of the reversible behavior at the fast scan rates. This scaled slow scan rate data was subtracted from the distorted scan. In all cases, ν_{slow} is the 20 mV/s scan, where there is no convective interference with the voltammetry as demonstrated by digital simulation of the cyclic voltammetry at that scan rate. Figure 4a shows an overlay of the residual current resulting from the data subtraction for the prefeature at 2000 mV/s under both H₂O and D₂O conditions. The subtracted prefeature undergoes the same shift as the diffusive wave upon deuteration; however, as shown in Figure 4b, it scales linearly with scan rate, as would be expected of an adsorbed species. A Nernstian adsorbate layer follows the equation⁴⁷

$$i_p = \frac{n^2 F^2}{4RT} \nu \Gamma_O^* \quad [7]$$

It is noted that for electrodes with the same surface area, the slope depends only on standard constants and the surface coverage Γ_O^* . Because the slopes of Figure 4b agree within a 95% confidence limit, it can be stated that the surface species in these cases have the same value of Γ_O^* , as would be expected for H_{ads} and D_{ads}.

In further support of the assertion that this voltammetric feature is the H_{ads} species, careful analysis of the thermodynamic data presented in Scheme 1 predicts that an H_{ads} should occur at -0.475 V vs. SCE , the same as the experimentally observed potential for the prefeature, which occurs at -0.485 V vs. SCE at 2000 mV/s, as shown in Figure 4a. Taking the reverse of path i, 2.2 kcal/mol can be converted to a potential scale via Faraday's constant to give 0.095 V. This can then be added to path iv, which is predicted to occur thermodynamically at -0.57 V . The addition of these two values gives a potential of -0.475 V vs. SCE , which coincides with the potential of the prefeature, lending support to the assignment of this feature as a H_{ads} intermediate.

This analysis of the system supports the presence of an H_{ads} intermediate in the proton reduction of weak acids at platinum electrodes. The fact that the purely thermodynamic data strongly supports this conclusion suggests that this reduction is not kinetically limited.

Methods

Computational methods.— Density functional theory (DFT) calculations were carried out at the gradient-corrected PBE level of theory³⁶ within the plane-wave pseudopotential scheme as

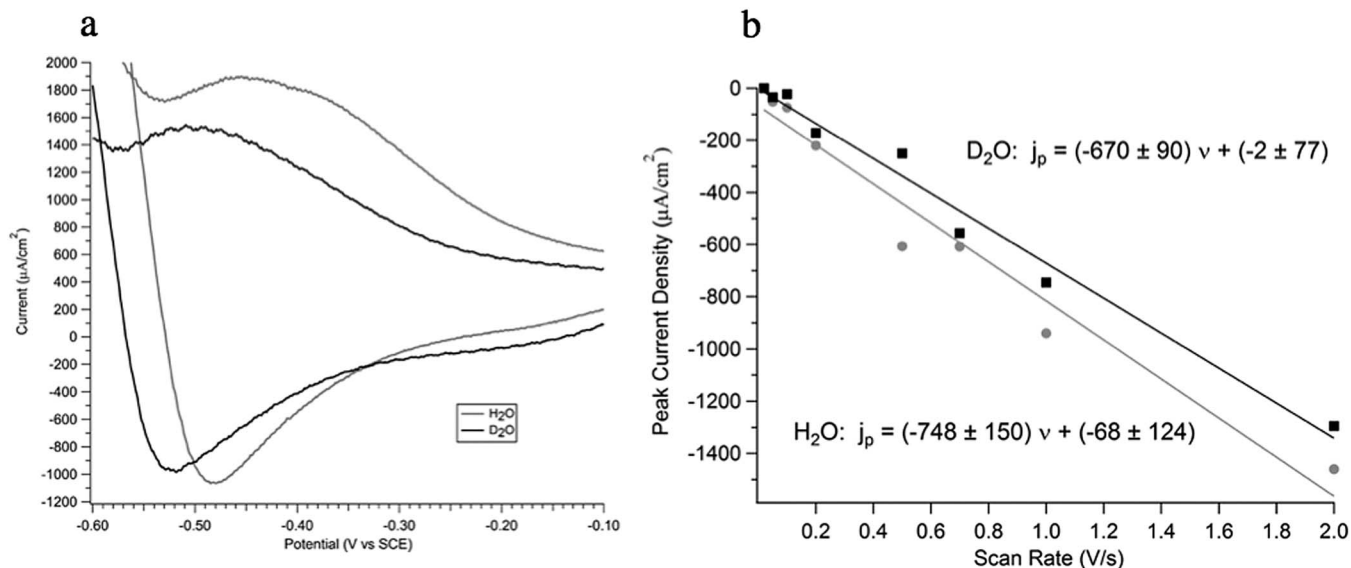


Figure 4. a) adsorptive peak obtained via subtraction of scaled cyclic voltammograms from 2000 mV/s scan. b) linear response of peak reduction potential with scan rate.

implemented in the Quantum ESPRESSO⁴⁸ software package to model Pt(111) surface similar to our previous work.¹⁹ Two significant differences from our prior work are that (i) the Pt(111) surface was modeled by a periodically repeating 3×3 supercell ($8.47 \text{ \AA} \times 8.47 \text{ \AA}$) in a four-layer slab where the two bottom layers were fixed at the optimized bulk lattice constants and (ii) as the Pt(111) surface is expected to have near 1 ML hydrogen ad-atom coverage at fcc sites at the experimental conditions, a surface coverage of 8/9 is chosen for the calculations. The Monkhorst-Pack type of \mathbf{k} -point sampling with a $2 \times 2 \times 1$ grid was chosen for the slab calculations and the convergence in binding energies were further checked by employing denser \mathbf{k} -point grids of $3 \times 3 \times 1$ and $6 \times 6 \times 1$. Select geometries for the cluster calculations were fully optimized at the PBE level of density functional theory³⁶ using the Stuttgart ECP60MWB contracted pseudopotential basis set⁴⁹ for Pt and the 6-31G(d) basis set⁵⁰ for all other atoms. The grid = ultrafine option (in Gaussian 09)⁵¹ was chosen for integral evaluation and an automatically generated density-fitting basis set was used within the resolution-of-the-identity approximation for the evaluation of Coulomb integrals. Solvation effects associated with water as solvent were accounted for by using the SMD aqueous continuum solvation model.⁵² The aqueous solvation contribution to the plane-wave-based periodic DFT optimized structures were calculated via generating model clusters with 14 Pt atoms and performing single point calculations at the PBE level of density functional theory using SDD basis set for Pt and the 6-311+G(2df, p) basis set for all other atoms while restricting the spin state of model structures to open-shell singlet or doublet states. The equilibrium isotope effect (EIE) associated with deuterium exchange of acidic hydrogen of PyrH^+ is predicted via performing phonon calculations at the $q = \Gamma$ point only to obtain the vibrational frequencies associated with the H ad-atom and PyrH^+ on a Pt(111) fcc site. The vibrational frequencies are used to calculate the changes in ZPE and entropic contributions due to H/D exchange, which in turn are employed to predict the EIE. Further details on computational methods are available in the supporting information.

Materials.— Supporting electrolyte KCl (EMD, 99%) was dried in a vacuum oven at 100°C for at least 3 hours prior to experiment and mixed at 0.5 M concentration with either deionized water or D_2O (Cambridge Isotope Labs, 99.9%). Pyridine (Sigma Aldrich, 99.8%), potassium acetate (Alfa Aesar, 99%), sodium benzoate (JT Baker), 2,6-lutidine (Sigma Aldrich, 98%) and 4-methylpyridine

(Sigma Aldrich, 98%) were used in 10 mM concentration at their $\text{pH} = \text{pKa}$ or $\text{pD} = \text{pKa(D)}$, for a bulk protonated (deuterated) acid concentration of 5 mM or for examination of peak currents, at $\text{pH} = \text{pH}^* = 3.0$. Pyridine was distilled over calcium hydride. All solid analytes were dried in a vacuum oven at 100°C for at least 3 hours prior to use. 4-methylpyridine and 2,6-lutidine were used as received.

Cyclic voltammetry.— Cyclic voltammograms were recorded on either CHI 760 or CHI 1140 potentiostats with instrument error of less than 5 mV. Saturated calomel (SCE) reference half cells (Accumet), Pt mesh counter electrodes and Pt disk working electrodes (BASi, 0.020 cm^2 area) were used in a standard 3 electrode configuration. The working electrode was cleaned between each scan rate by polishing with $1 \mu\text{m}$ alumina particles (Fisher) on cloth pads. Glassware was dried in a 100°C oven for at least 30 minutes prior to use. Solutions were purged with Ar to exclude O_2 . The pH reading in D_2O solution of a standard pH meter calibrated in pH 4, 7 and 10 H_2O -based buffers (Fisher), termed pH^* , was adjusted to the pKa of the acid as measured in H_2O (for pyridine, adjusted $\text{pH}^* = \text{pKa(H)} = 5.2$) using 0.1 M DCl (Aldrich, 99.9%) in D_2O . According to the formula in Krężel, for the acids in question this should result in a pD and pKa(D) values shifted by 0.4 pH units, (for pyridinium, $\text{pD} = \text{pKa(D)} = 5.63$). For evaluation of the cyclic voltammetric peak current in pyridinium reduction, pH or pH^* of the solution was adjusted to 3.0, where 99% of the analyte is protonated. Scan rates of 5–2000 mV/s were recorded.

Rotating disk voltammetry.— Rotating disk voltammograms were recorded on a CHI 760 potentiostat. Saturated calomel (SCE) reference half cells (Accumet), Pt mesh counter electrodes and Pt disk working electrodes (Pine, 0.196 cm^2 area) were used in a standard 3 electrode configuration. Rotation of the working electrode was controlled by a MSRZ Analytical Rotator (Pine). Rotation rates of 200–2500 rpm were used. The working electrode was cleaned between each scan rate by polishing with $1 \mu\text{m}$ alumina particles (Fisher) on cloth pads. Glassware was dried in a 100°C oven for at least 30 minutes prior to use. Solutions were purged with Ar to exclude O_2 . For the n and D calculation, all cyclic voltammograms as well as the rotating disk voltammograms were recorded in the same solution and with the same electrode. The pH^* was adjusted to 3.0 in order to ensure that all changes in current were related to deuteration rather than changes in bulk concentration of pyridinium.

Conclusions

An isotopic shift in the potential of the cathodic wave of -25 mV when comparing PyrD^+ in D_2O to PyrH^+ in H_2O was observed in cyclic voltammetry at a platinum electrode. The agreement between the experimentally observed potential shift in cyclic voltammetry for a number of weak acids, the expected potential shifts of the weak acids due to the lower pK_a of the catalyst upon deuteration, and the DFT calculated shift due to deuteration of PyrH^+ support the mechanistic hypothesis that the reduction of PyrH^+ in water at a Pt electrode produces H_{ads} , with the pK_a of PyrH^+ governing the cathodic potential. This mechanism indicates that high Brønsted acid concentration leading to surface hydride formation may be an important paradigm in CO_2 reduction in addition to its well-known role in proton reduction. Ongoing experimental work is assessing whether the H_{ads} species formed in weak acid reductions on Pt are susceptible to electrophilic attack by CO_2 and thereby transfer to CO_2 by proton coupled hydride transfer as suggested by earlier studies.¹⁸

Acknowledgments

VS acknowledges support from the AFOSR grant # FA9550-13-1-0020 and supercomputing time from NERSC and from the high-performance computing facilities at Yale University. MZE was funded by a Computational Materials and Chemical Sciences (CMCSN) project at Brookhaven National Laboratory under contract DE-AC02-98CH10886 with the U.S. Department of Energy and supported by its Division of Chemical Sciences, Geosciences & Biosciences, Office of Basic Energy Sciences. ABB acknowledges support from the Air Force Office of Scientific Research through the MURI program under AFOSR Award No. FA9550-10-1-0572 and the NSF under award CHE-1308652. ELZ is supported in part by the Department of Energy Office of Science Graduate Fellowship Program (DOE SCGF), made possible in part by the American Recovery and Reinvestment Act of 2009, administered by ORISE-ORAU under contract no. DE-AC05-06OR23100.

References

- B. Kumar, M. Llorente, J. Froehlich, T. Dang, A. Sathrum, and C. P. Kubiak, "Photochemical and Photoelectrochemical Reduction of CO_2 ," *Annu. Rev. Phys. Chem.*, **63**, 541 (2012).
- E. E. Benson, C. P. Kubiak, A. J. Sathrum, and J. M. Smieja, "Electrocatalytic and Homogeneous Approaches to Conversion of CO_2 to Liquid Fuels," *Chem. Soc. Rev.*, **38**, 89 (2009).
- C. Costentin, M. Robert, and J.-M. Savéant, "Catalysis of the Electrochemical Reduction of Carbon Dioxide," *Chem. Soc. Rev.*, **42**, 2423 (2013).
- Y. Oh and X. Hu, "Organic Molecules as Mediators and Catalysts for Photocatalytic and Electrocatalytic CO_2 Reduction," *Chem. Soc. Rev.*, **42**, 2253 (2013).
- A. J. Morris, G. J. Meyer, and E. Fujita, "Molecular Approaches to the Photocatalytic Reduction of Carbon Dioxide for Solar Fuels," *Acc. Chem. Res.*, **42**, 1983 (2009).
- C. E. Barton, P. S. Lakkaraju, and D. M. Rampulla, A. J. Morris, E. Abelev, and A. B. Bocarsly, "Using a One-Electron Shuttle for the Multielectron Reduction of CO_2 to Methanol: Kinetic, Mechanistic, and Structural Insights," *J. Am. Chem. Soc.*, **132**, 11539 (2010).
- G. Seshadri, C. Lin, and A. B. Bocarsly, "A New Homogeneous Electrocatalyst for the Reduction of Carbon Dioxide to Methanol at Low Overpotential," *J. Electroanal. Chem.*, **372**, 145–150 (1994).
- A. J. Morris, R. T. McGibbon, and A. B. Bocarsly, "Electrocatalytic Carbon Dioxide Activation: The rate-determining step of pyridinium-catalyzed CO_2 reduction," *ChemSusChem*, **4**, 191 (2011).
- E. E. Barton, D. M. Rampulla, and A. B. Bocarsly, "Selective Solar-Driven Reduction of CO_2 to Methanol Using a Catalyzed p-GaP Based Photoelectrochemical Cell," *J. Am. Chem. Soc.*, **130**, 6342 (2008).
- D. J. Boston, C. Xu, D. W. Armstrong, and F. M. MacDonnell, "Photochemical Reduction of Carbon Dioxide to Methanol and Formate in a Homogeneous System with Pyridinium Catalysts," *J. Am. Chem. Soc.*, **135**, 16252 (2013).
- Y. Yan, E. L. Zeitler, J. Gu, Y. Hu, and A. B. Bocarsly, "Electrochemistry of Aqueous Pyridinium: Exploration of a Key Aspect of Electrocatalytic Reduction of Carbon Dioxide to Methanol," *J. Am. Chem. Soc.*, **135**, 14020 (2013).
- M. Z. Kamrath, R. A. Relph, and M. A. Johnson, "Vibrational Predissociation Spectrum of the Carbamate Radical Anion, $\text{C}_5\text{H}_5\text{N-CO}_2^-$, Generated by Reaction of Pyridine with $(\text{CO}_2)^{\text{m-}}$," *J. Am. Chem. Soc.*, **132**, 15508 (2010).
- J. A. Keith and E. A. Carter, "Theoretical Insights into Pyridinium-Based Photoelectrocatalytic Reduction of CO_2 ," *J. Am. Chem. Soc.*, **134**, 7580 (2012).
- J. A. Keith and E. A. Carter, "Electrochemical Reactivities of Pyridinium in Solution: Consequences for CO_2 Reduction Mechanisms," *Chem. Sci.*, **4**, 1490 (2013).
- C.-H. Lim, A. M. Holder, and C. B. Musgrave, "The Mechanism of Homogeneous Reduction of CO_2 by Pyridine: Proton Relay in Aqueous Solvent and Aromatic Stabilization," *J. Am. Chem. Soc.*, **135**, 142 (2012).
- C. Costentin, J. C. Canales, B. Haddou, and J.-M. Savéant, "Electrochemistry of Acids on Platinum. Application to the Reduction of Carbon Dioxide in the Presence of Pyridinium Ion in Water," *J. Am. Chem. Soc.*, **135**, 17671 (2013).
- A. J. Lucio and S. K. Shaw, "Pyridine and Pyridinium Electrochemistry on Polycrystalline Gold Electrodes and Implications for CO_2 Reduction," *J. Phys. Chem. C*, **119**, 12523 (2015).
- E. Lebègue, J. Agullo, M. Morin, and D. Bélanger, "The Role of Surface Hydrogen Atoms in the Electrochemical Reduction of Pyridine and CO_2 in Aqueous Electrolyte," *ChemElectroChem*, **1**, 1013 (2014).
- M. Z. Ertem, S. J. Konezny, C. M. Araujo, and V. S. Batista, "Functional Role of Pyridinium during Aqueous Electrochemical Reduction of CO_2 on Pt(111)," *J. Phys. Chem. Lett.*, **4**, 745 (2013).
- C. Canhoto, M. Matos, A. Rodrigues, M. D. Geraldo, and M. F. Bento, "Voltammetric Analysis of Weak Acids with Microelectrodes," *J. Electroanal. Chem.*, **570**, 63 (2004).
- A. Peremans and A. Tadjeddine, "Electrochemical Deposition of Hydrogen on Platinum Single Crystals Studied by Infrared-Visible Sum-Frequency Generation," *J. Chem. Phys.*, **103**, 7197 (1995).
- Z.-Q. Tian and B. Ren, "Adsorption and Reaction at Electrochemical Interfaces as Probed by Surface-Enhanced Raman Spectroscopy," *Annu. Rev. Phys. Chem.*, **55**, 197 (2004).
- B. E. Conway and G. Jerkiewicz, "Nature of Electrosorbed H and its Relation to Metal Dependence of Catalysis in Cathodic H_2 Evolution," *Solid State Ionics*, **150**, 93 (2002).
- B. Ren, X. Xu, X. Q. Li, W. B. Cai, and Z. Q. Tian, "Extending Surface Raman Spectroscopic Studies to Transition Metals for Practical Applications: II. Hydrogen Adsorption at Platinum Electrodes," *Surf. Sci.*, **427-428**, 157–161 (1999).
- A. Zolfaghari, M. Chayer, and G. Jerkiewicz, "Energetics of the Underpotential Deposition of Hydrogen on Platinum Electrodes: I. Absence of Coadsorbed Species," *J. Electrochem. Soc.*, **144**, 3034 (1997).
- J. Clavilier and D. Armand, "Electrochemical Induction of Changes in the Distribution of the Hydrogen Adsorption States on Pt (100) and Pt (111) Surfaces in Contact with Sulphuric Acid Solution," *J. Electroanal. Chem. Interfacial Electrochem.*, **199**, 187 (1986).
- J. Barber, S. Morin, and B. E. Conway, "Specificity of the Kinetics of H_2 Evolution to the Structure of Single-Crystal Pt Surfaces, and the Relation between OPD and UPD H," *J. Electroanal. Chem.*, **446**, 125 (1998).
- B. E. Conway, J. Barber, and S. Morin, "Comparative Evaluation of Surface Structure Specificity of Kinetics of UPD and OPD of H at Single-Crystal Pt Electrodes," *Electrochim. Acta*, **44**, 1109 (1998).
- E. Skulason, G. S. Karlberg, J. Rossmeisl, T. Bligaard, J. Greeley, H. Jonsson, and J. K. Nørskov, "Density Functional Theory Calculations for the Hydrogen Evolution Reaction in an Electrochemical Double Layer on the Pt(111) Electrode," *Phys. Chem. Chem. Phys.*, **9**, 3241–3250 (2007).
- E. Skulason, V. Tripkovic, M. E. Bjorketun, S. Gudmundsdottir, G. Karlberg, J. Rossmeisl, T. Bligaard, H. Jonsson, and J. K. Nørskov, "Modeling the Electrochemical Hydrogen Oxidation and Evolution Reactions on the Basis of Density Functional Theory Calculations," *J. Phys. Chem. C*, **114**, 18182 (2010).
- N. Nanbu, F. Kitamura, T. Ohsaka, and K. Tokuda, "Adsorption of Atomic Hydrogen on a Polycrystalline Pt Electrode Surface Studied by FT-IRAS: the Influence of Adsorbed Carbon Monoxide on the Spectral Feature," *J. Electroanal. Chem.*, **485**, 128 (2000).
- W. C. Barrette, H. W. Johnson and D. T. Sawyer, "Voltammetric Evaluation of the Effective Acidities (pK_a) for Brønsted Acids in Aprotic Solvents," *Anal. Chem.*, **56**, 1890–1898 (1984).
- K. B. Wiberg, "The Deuterium Isotope Effect," *Chem. Rev.*, **55**, 713 (1955).
- M. Ciszowska, Z. Stojek, and J. G. Osteryoung, "Voltammetric Reduction of Polyprotic Acids at the Platinum Microelectrode: Dependence on Supporting Electrolyte," *J. Electroanal. Chem.*, **398**, 49 (1995).
- M. Ciszowska, Z. Stojek, S. E. Morris, and J. G. Osteryoung, "Steady-State Voltammetry of Strong and Weak Acids with and without Supporting Electrolyte," *Anal. Chem.*, **64**, 2372 (1992).
- J. P. Perdew, K. Burke, and M. Ernzerhof, "Generalized Gradient Approximation Made Simple," *Phys. Rev. Lett.*, **77**, 3865 (1996).
- A. Krężel and W. Bal, "A formula for correlating pK_a values determined in D_2O and H_2O ," *Journal of Inorganic Biochemistry*, **98**, 161 (2004).
- G. N. Lewis and P. W. Schutz, "The Ionization of Some Weak Electrolytes in Heavy Water," *J. Am. Chem. Soc.*, **56**, 1913 (1934).
- E. L. Wehry and L. B. Rogers, "Deuterium Isotope Effects on the Protolytic Dissociation of Organic Acids in Electronically Excited States," *J. Am. Chem. Soc.*, **88**, 351 (1966).
- I. R. Bellobono and P. Beltrame, "Isotope Effects on Acid-Base Equilibria of Pyridine and $[\text{}^2\text{H}_5]\text{pyridine}$ in Protium and in Deuterium Oxide," *J. Chem. Soc. B*, **0**, 620 (1969).
- R. A. Robinson, M. Paabo, and R. G. Bates, "Deuterium Isotope Effect on the Dissociation of Weak Acids in Water and Deuterium Oxide," *J. Res. Nat. Bur. Stan.*, **73A**, 299 (1968).

42. In *CRC Handbook of Chemistry and Physics*, W. M. Haynes, Ed. CRC Press/Taylor and Francis: Boca Raton, FL, (2011).
43. D. E. Morris and W. H. Smith, "Direct Voltammetric Determination of the Equilibrium Isotope Effect in Naphthalene-h8/d8, Anthracene-h10/d10, and Benzophenone-12CO/13CO." *Journal of the Electrochemical Society*, **138**, 1351 (1991).
44. R. S. Nicholson and I. Shain, "Theory of Stationary Electrode Polarography." *Anal. Chem.*, **36**, 706 (1964).
45. P. Vanýsek, "Ionic conductivity and Diffusion at Infinite Dilution." In *CRC Handbook of Chemistry and Physics*, W. M. Haynes, Ed. CRC Press/Taylor and Francis: Boca Raton, FL, (2011).
46. G. N. Lewis and T. C. Doody, "The mobility of ions in H²H₂O." *J. Am. Chem. Soc.*, **55**, 3504 (1933).
47. A. J. Bard and L. R. Faulkner, "Electroactive Layers and Modified Electrodes." *Electrochemical Methods: Fundamentals and Applications*. Second Edition, John Wiley & Sons, Inc. New York, 2001, pp 591.
48. P. Giannozzi, S. Baroni, N. Bonini, M. Calandra, R. Car, C. Cavazzoni, D. Ceresoli, G. L. Chiarotti, M. Cococcioni, I. Dabo, A. Dal Corso, S. de Gironcoli, S. Fabris, G. Fratesi, R. Gebauer, U. Gerstmann, C. Gougoussis, A. Kokalj, M. Lazzeri, L. Martin-Samos, N. Marzari, F. Mauri, R. Mazzarello, S. Paolini, A. Pasquarello, L. Paulatto, C. Sbraccia, S. Scandolo, G. Sclauzero, A. P. Seitsonen, A. Smogunov, P. Umari, and R. M. Wentzcovitch, "QUANTUM ESPRESSO: a modular and open-source software project for quantum simulations of materials." *J. Phys.: Condens. Matter*, **21** (2009).
49. D. Andrae, U. Haussermann, M. Dolg, H. Stoll, and H. Preuss, "Energy-Adjusted Ab Initio Pseudopotentials for the 2nd and 3rd Row Transition-Elements." *Theoretica Chimica Acta*, **77**, 123 (1990).
50. W. J. Hehre, L. Radom, P. V. R. Schleyer, and J. A. Pople, *Ab Initio Molecular Orbital Theory*. Wiley: New York, 1986.
51. M. J. Frisch, G. W. Trucks, H. B. Schlegel, G. E. Scuseria, M.A. Robb, J. R. Cheeseman, G. Scalmani, V. Barone, B. Mennucci, G. A. Petersson, H. Nakatsuji, M. Caricato, X. Li, H. P. Hratchian, A. F. Izmaylov, J. Bloino, G. Zheng, J. L. Sonnenberg, M. Hada, M. Ehara, K. Toyota, R. Fukuda, J. Hasegawa, M. Ishida, T. Nakajima, Y. Honda, O. Kitao, H. Nakai, T. Vreven, J. A. Montgomery, J. E. Peralta, F. Ogliaro, M. Bearpark, J. J. Heyd, E. Brothers, K. N. Kudin, V. N. Staroverov, R. Kobayashi, J. Normand, K. Raghavachari, A. Rendell, J. C. Burant, S. S. Iyengar, J. Tomasi, M. Cossi, N. Rega, J. M. Millam, M. Klene, J. E. Knox, J. B. Cross, V. Bakken, C. Adamo, J. Jaramillo, R. Gomperts, R. E. Stratmann, O. Yazyev, A. J. Austin, R. Cammi, C. Pomelli, J. W. Ochterski, R. L. Martin, K. Morokuma, V. G. Zakrzewski, G. A. Voth, P. Salvador, J. J. Dannenberg, S. Dapprich, A. D. Daniels, Ö. Farkas, J. B. Foresman, J. V. Ortiz, J. Cioslowski, and D. J. Fox, Gaussian 09, Revision A.02. Gaussian, Inc.: Wallingford, CT, 2010.
52. A. V. Marenich, C. J. Cramer, and D. G. Truhlar, "Universal Solvation Model Based on Solute Electron Density and a Continuum Model of the Solvent Defined by the Bulk Dielectric Constant and Atomic Surface Tensions." *J. Phys. Chem. B*, **113**, 6378 (2009).